SUPPLEMENT TO THE NCEP CLIMATE FORECAST SYSTEM REANALYSIS

BY SURANJANA SAHA, SHRINIVAS MOORTHI, HUA-LU PAN, XINGREN WU, JIANDE WANG, SUDHIR NADIGA, PATRICK TRIPP, ROBERT KISTLER, JOHN WOOLLEN, DAVID BEHRINGER, HAIXIA LIU, DIANE STOKES, ROBERT GRUMBINE, GEORGE GAYNO, JUN WANG, YU-TAI HOU, HUI-YA CHUANG, HANN-MING H. JUANG, JOE SELA, MARK IREDELL, RUSS TREADON, DARYL KLEIST, PAUL VAN DELST, DENNIS KEYSER, JOHN DERBER, MICHAEL EK, JESSE MENG, HELIN WEI, RONGQIAN YANG, STEPHEN LORD, HUUG VAN DEN DOOL, ARUN KUMAR, WANQIU WANG, CRAIG LONG, MUTHUVEL CHELLIAH, YAN XUE, BOYIN HUANG, JAE-KYUNG SCHEMM, WESLEY EBISUZAKI, ROGER LIN, PINGPING XIE, MINGYUE CHEN, SHUNTAI ZHOU, WAYNE HIGGINS, CHENG-ZHI ZOU, QUANHUA LIU, YONG CHEN, YONG HAN, LIDIA CUCURULL, RICHARD W. REYNOLDS, GLENN RUTLEDGE, AND MITCH GOLDBERG

AFFILIATIONS: SAHA, MOORTHI, PAN, BEHRINGER, STOKES, GRUMBINE, HOU, CHUANG, JUANG, SELA, IREDELL, TREADON, KEYSER, DERBER, EK, AND LORD—Environmental Modeling Center, NCEP/NWS/NOAA, Camp Springs, Maryland; VAN DEN DOOL, KUMAR, W. WANG, LONG, CHELLIAH, XUE, SCHEMM, EBISUZAKI, XIE, CHEN, AND HIGGINS—Climate Prediction Center, NCEP/NWS/NOAA, Camp Springs, Maryland; WU, JI. WANG, NADIGA, KISTLER, WOOLLEN, H. LIU, GAYNO, JU. WANG, KLEIST, VAN DELST, MENG, WEI, AND YANG—Science Applications International Corporation (SAIC), McLean, Virginia; ZOU, CHEN, HAN, CUCURULL, AND GOLDBERG—Center for Satellite Applications and Research, NESDIS/NOAA, Camp Springs, Maryland; Q. LIU—Joint Center for Satellite Data Assimilation, NASA–NOAA, Camp Springs, Maryland; RUTLEDGE—NOAA/NESDIS/National Climatic Data Center, Asheville, North Carolina; TRIPP—Plurality Engineering and Scientific Solutions, LLC, Columbia, Maryland; REYNOLDS—Cooperative Institute for Climate & Satellites, NOAA, Camp Springs, Maryland and North Carolina State University, Raleigh, North Carolina; HUANG, LIN, AND ZHOU—Wyle Information System, McLean, Virginia

CORRESPONDING AUTHOR: Dr. Suranjana Saha, NOAA Science Center, 5200 Auth Road, Camp Springs, MD 20746
E-mail: suranjana.saha@noaa.gov

DOI: 10.1175/2010BAMS3001.2

In final form 12 April 2010

The sections in this paper are supplemental to Saha et al. (2010). The "Performance of Observing Systems" section is a collection of figures that highlight the performance of different observing systems in the CFSR, the "Satellite Bias Correction Spin Up for CFSR (expanded from Saha et al. 2010)" section explains in detail how the bias corrections were obtained when new satellites were spun up in the CFSR, the "Data Access" section describes the points of access to this massive dataset, and the appendix describes some of the datasets available.

PERFORMANCE OF OBSERVING SYSTEMS. Figures S1–S22 illustrate the observing system performances of a number of data types used in the Climate Forecast System Reanalysis (CFSR), with respect to the quality control reactions and the monthly RMS and mean fits to the analysis and first-guess backgrounds over the 31-yr period from 1979 to 2009. Details of the chart legends are found in the captions for Figs. S1 and S17. Some specific details about the conventional observing systems used in the CFSR and their sources, characteristics, and preparation have been discussed in the "Conventional Observing Systems in the CFSR"

section of Saha et al. (2010). A complete set of performance charts can be viewed online (available at http://cfs.ncep.noaa.gov/cfsr).

The CFSR uses the National Centers for Environmental Protection (NCEP) operational observation quality control procedures, which are summarized in Table S1.

SATELLITE BIAS CORRECTION SPIN UP FOR CFSR (expanded from the main paper). This CFSR covers the period from 1979 to 2009. During these 31 years, a series of National Oceanic and Atmospheric Administration (NOAA)

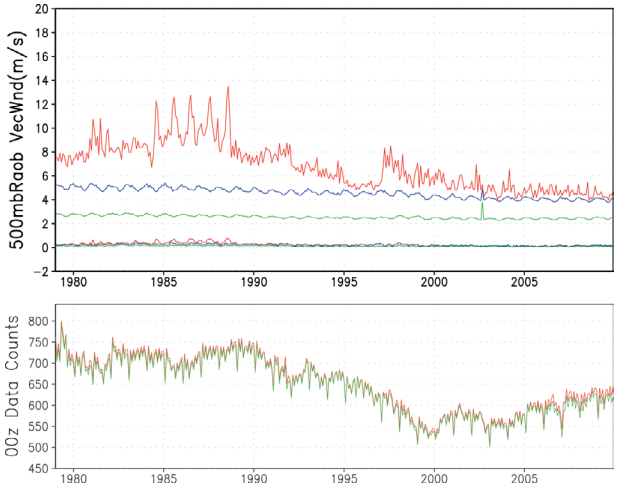

Fig. S1. Performance of 500-mb radiosonde wind observations. (top) Monthly RMS and mean fits of quality controlled observations to the first guess (blue) and the analysis (green). The fits of all observations, including those rejected by the quality control (QC), are shown (red). (bottom) The 0000 UTC data counts of all observations (red) and those that passed QC and were assimilated (green).

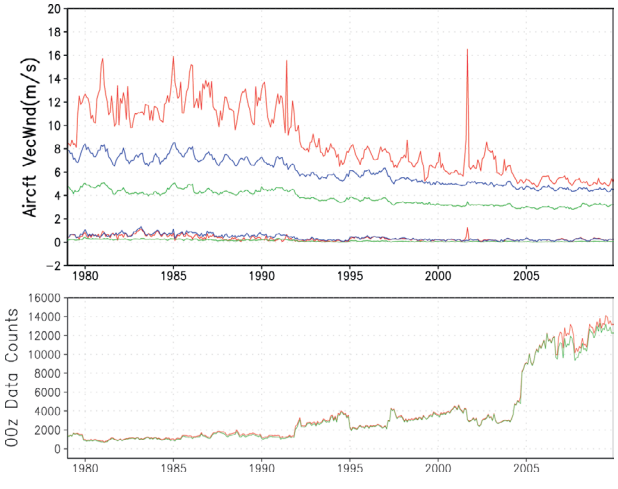

Fig. S2. As in Fig. S1, but for aircraft wind data.

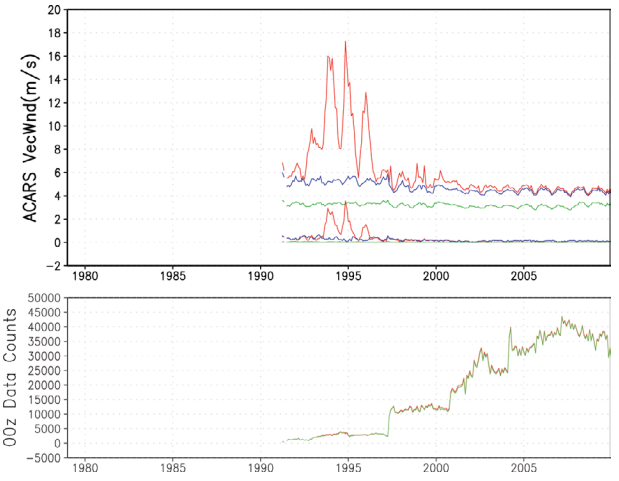

Fig. S3. As in Fig. S1, but for Aircraft Communications Addressing and Reporting System (ACARS) wind data.

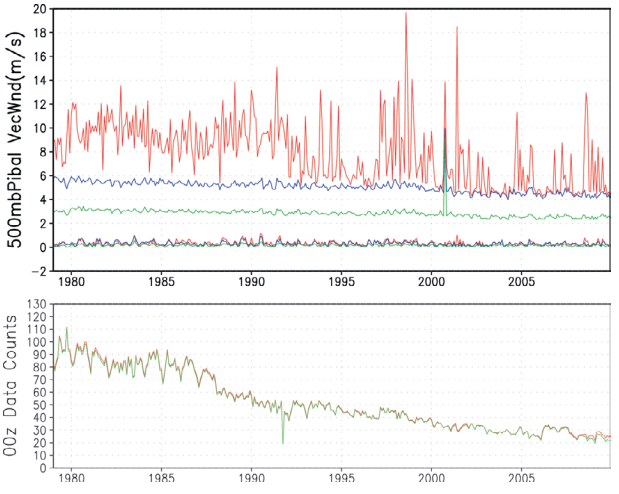

Fig. S4. As in Fig. S1, but for 500-mb pilot balloon wind.

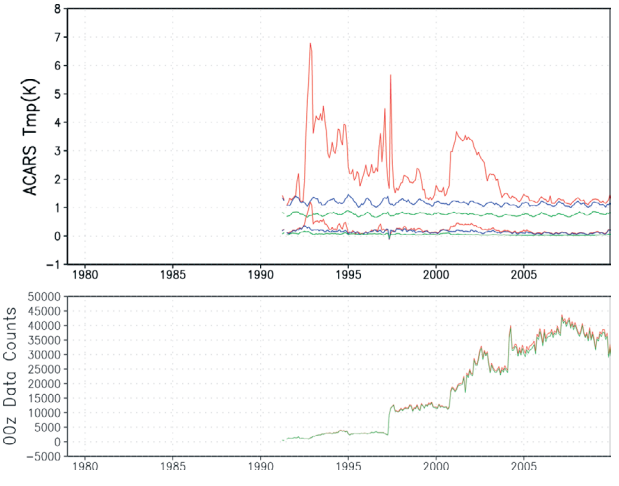

Fig. S5. As in Fig. S1, but for ACARS temperature data.

polar-orbiting satellites operated for certain periods of time (see Fig. 4 of Saha et al. 2010). The radiance measurements from these satellites were directly assimilated into the analysis system, which is one of the major improvements of the CFSR over the NCEP–Department of Energy (DOE) Reanalysis Global Reanalysis 2 (R2). Substantial biases exist when the radiance measurements are compared to the model-simulated radiances. These biases are complicated and related to instrument calibration, data processing, and deficiencies in the radiative transfer model. Accurate bias corrections for these satellite observations were required for the success of the CFSR. This section describes the method to estimate the biases of these historical satellite observations.

Table S1. NCEP operational observation quality control procedures.

Program	Purpose	Input file	Output file
PREVENTS	Store guess values Store observation error Ps gross check	SIGF06 PREPBUFR	PREPBUFR
ACQC	Aircraft QC track and duplicate check	PREPBUFR	PREPBUFR
ACAR_CQC	ACARS ascent and descent check	PREPBUFR	PREPBUFR
CQC	RAOB complex QC Radiation bias correction	PREPBUFR	PREPBUFR
CQCVAD	VAD wind complex QC	PREPBUFR	PREPBUFR
PROFCQC	Profiler complex QC	PREPBUFR	PREPBUFR
GSI	Nonlinear variational QC	PREPBUFR	CNVSTAT
POSTEVENT	Store variational QC results Store analysis values	SIGANL CNVSTAT PREPBUFR	PREPBUFR

A variational satellite bias correction scheme was introduced by Derber and Wu (1998) when direct assimilation of radiance began. This scheme has been continually developed at NCEP since then and is used in the gridded statistical interpolation (GSI) system adapted for the CFSR. Radiance bias is composed of two parts: the satellite scan angle–dependent bias (SATANG) and the airmass-dependent bias (BIASCR). The SATANG file is updated following the analysis step as the weighted average of the previous cycle's SATANG file (containing the bias) and the departure between the new radiance measurements o and the model-simulated radiances g, [i.e., $(o - g)$]. SATANG is allowed to evolve very slowly [the weight given to the new $(o - g)$ is 1/120]. The airmass bias prediction equation is the sum of five terms: a constant, 0.01, and four weighted predictor terms. The predictors are the solar zenith angle, the cloud liquid water (CLW, only applied to microwave instruments), the temperature lapse rate, and the square of the lapse rate. The predictor coefficients are calculated using

Fig. S6. As in Fig. S1, but for SYNOP surface pressure data.

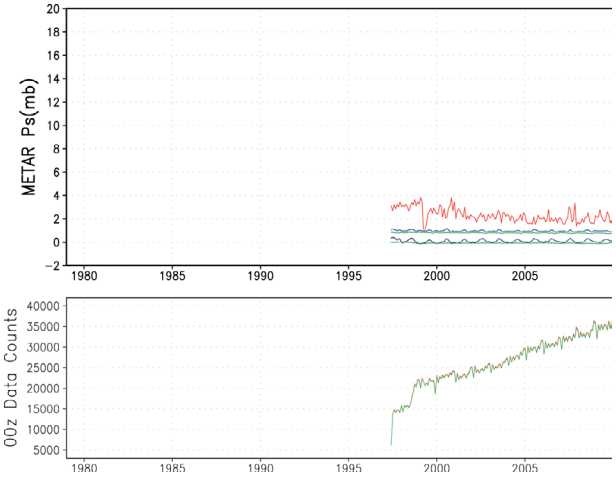

Fig. S7. As in Fig. S1, but for Meteorological Aviation Report (METAR) surface pressure data.

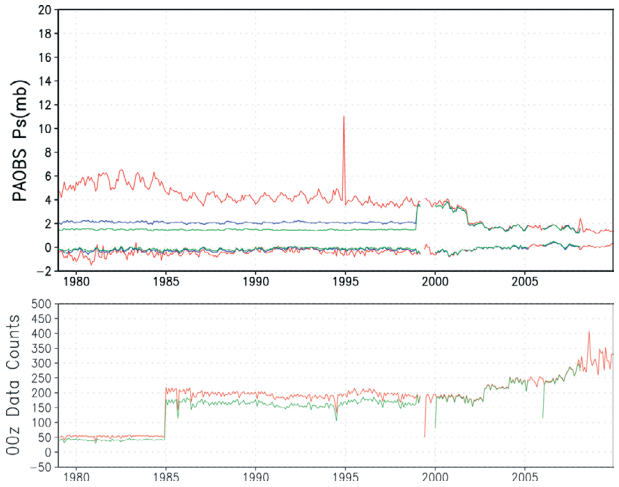

Fig. S8. As in Fig. S1, but for PAOB surface pressure data.

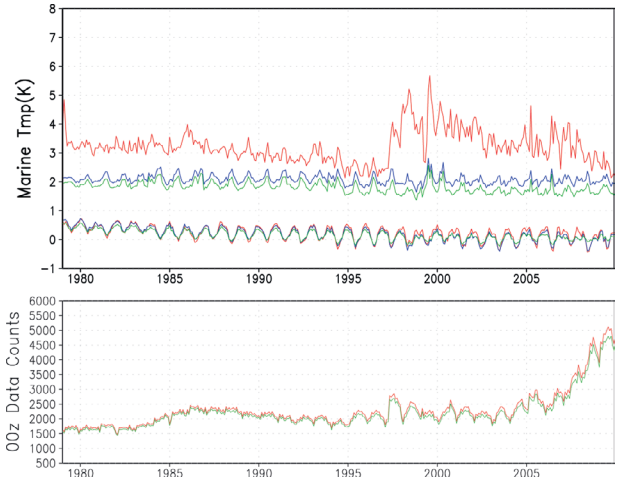

Fig. S9. As in Fig. S1, but for marine temperature data.

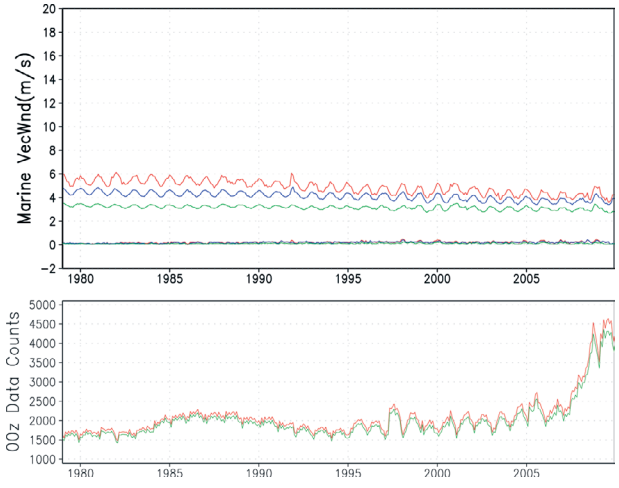

Fig. S10. As in Fig. S1, but for marine wind data.

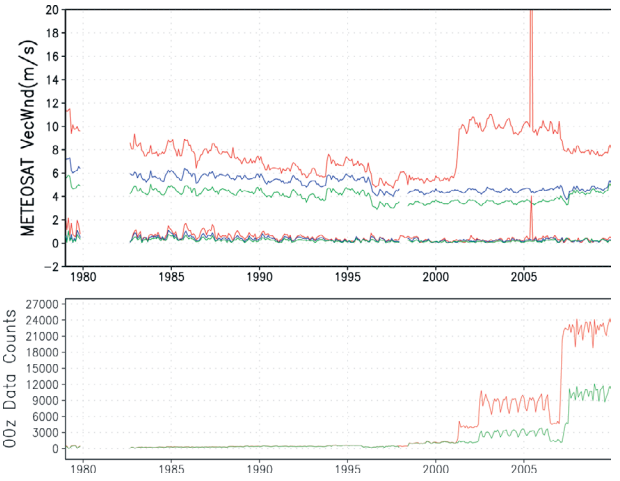

Fig. S11. As in Fig. S1, but for Meteosat satellite wind data.

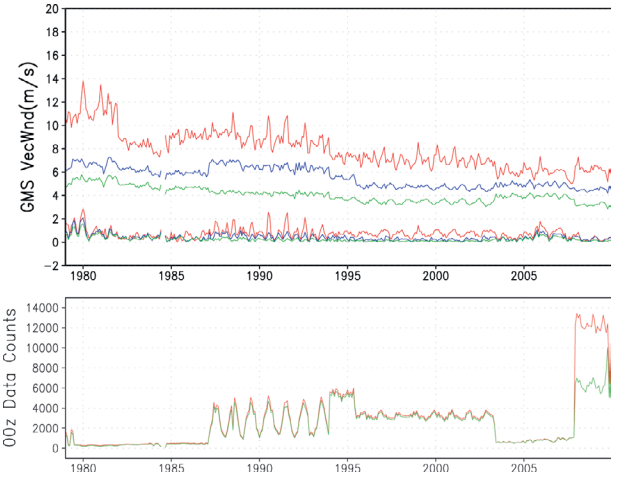

Fig. S12. As in Fig. S1, but for Geosynchronous Meteorological Satellite (GMS) satellite wind data.

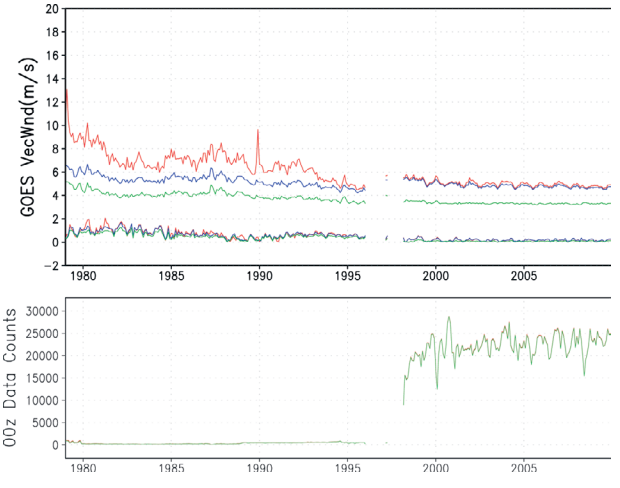

Fig. S13. As in Fig. S1, but for Geostationary Operational Environmental Satellite (GOES) satellite wind data.

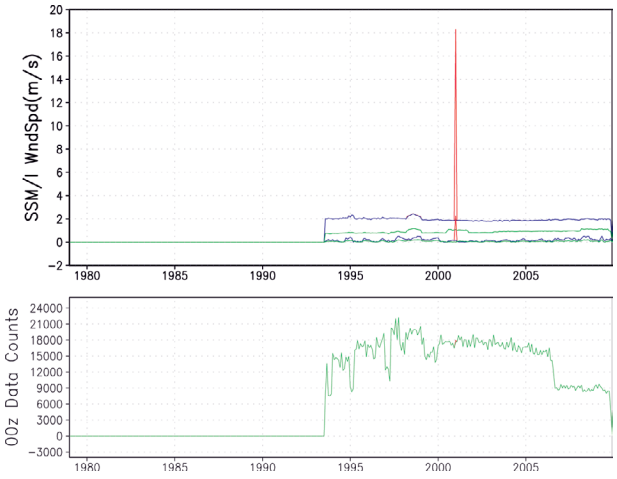

Fig. S14. As in Fig. S1, but for Special Sensor Microwave Imager (SSM/I)-derived wind speed data.

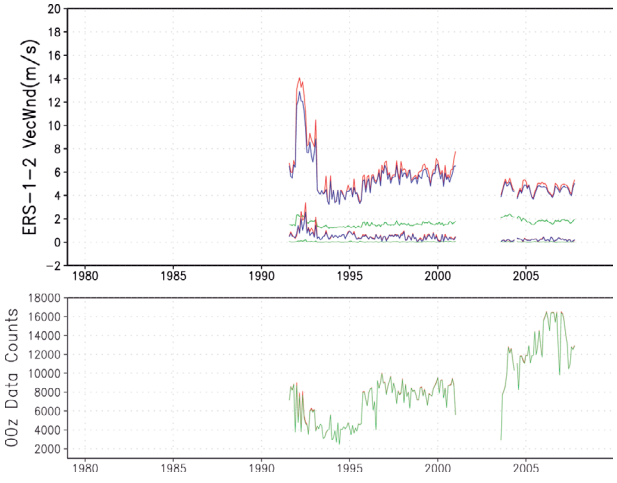

Fig. S15. As in Fig. S1, but for European Remote Sensing Satellite (ERS) ocean surface wind data.

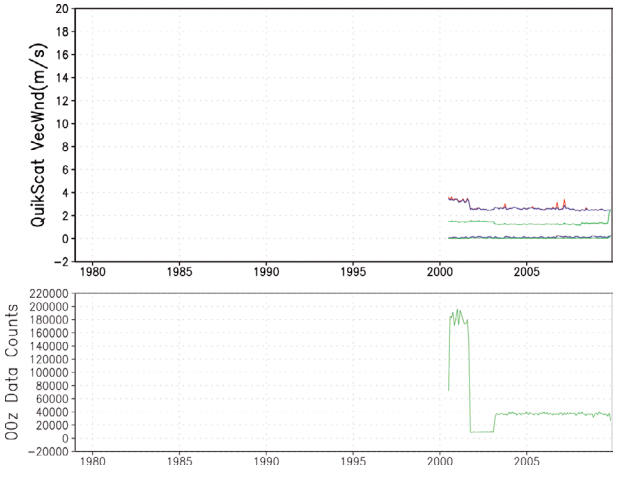

Fig. S16. As in Fig. S1, but for Quick Scatterometer (QuikSCAT) wind data.

the variational method (the predictor coefficients are additional analysis variables and are included in the minimization).

The biases from the historical satellite radiances can be estimated using a two-step procedure. First, the Global Data Assimilation System (GDAS) is run for a training period, starting from guess values, and the statistics of the ($o - g$) are collected throughout this training period. Second, the collected radiance statistics are then postprocessed to calculate a SATANG file. For a given scan position, channel, sensor, and satellite, the SATANG value is the average of the ($o - g$) weighted by the specified

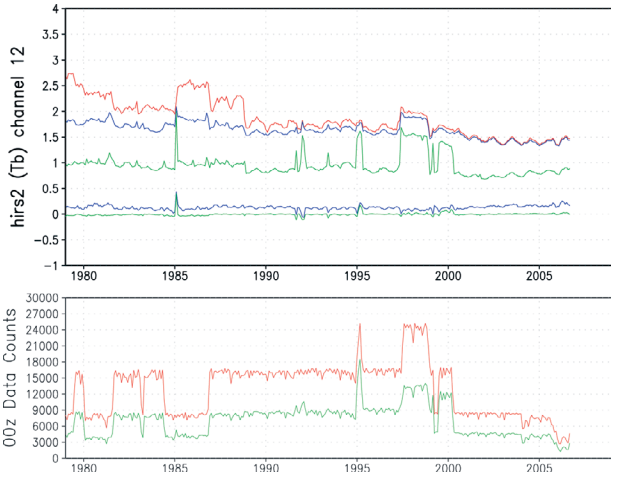

Fig. S17. Performance of HIRS-2 channel 12, which peaks at ~ 500 hPa. (top) The uncorrected rms ($o - g$) (red), bias-corrected ($o - g$) rms and mean (blue), and bias-corrected ($o - a$) rms and mean (green), where o is obs, a is analysis, and g is guess. (bottom) Total 0000 UTC counts (red) and accepted counts (green).

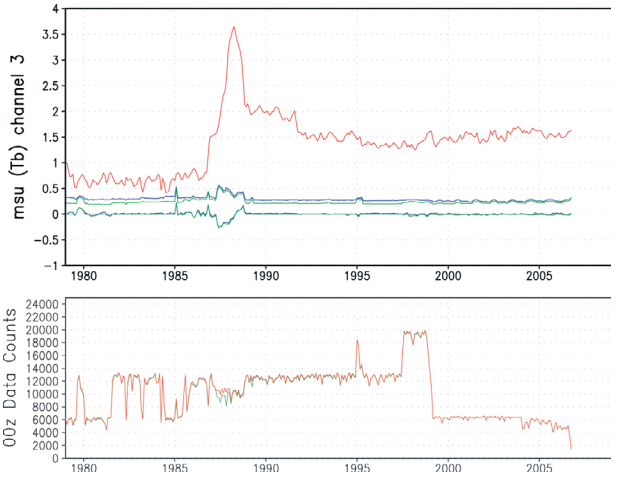

Fig. S18. As in Fig. S17, but for MSU channel 3, which peaks at ~ 300 hPa.

observation error inverse over the whole globe and the entire training period.

Table S2. List of experiments for the spinup of bias correction of historical satellites with their corresponding starting and ending times.

Satellite	Starting date	Ending date
N6-1	1979070100	1979100100
Television and Infrared Observation Satellite (TIROS)-N	1979010100	1979040100
NOAA-7	1981080100	1981120100
NOAA-8	1983050100	1983080100
NOAA-9	1985022500	1985060100
NOAA-6-2	1985101800	1986020100
NOAA-10	1986112600	1987030100
NOAA-11	1988110800	1989020100
NOAA-12	1991091600	1992010100
NOAA-14	1995010300	1995080100
NOAA-11-2, GOES-8, GOES-9	1997071500	1998010100
NOAA-15, GOES-10	1998091000	1999020100
AMSU-B NOAA-15	2000010600	2000040100
NOAA-16	2001012400	2001060100
GOES-12	2003040200	2003070100
GOES-11	2006062100	2006100100

Several preliminary experiments have been carried out to determine starting values and how long the training period should be. These experiments were run over the period from 2006110118 to 2007013018 using zeroed-out SATANG and BIASCR files. To simulate historical Microwave Sounder Unit (MSU) and High-Resolution Infrared Sounder Unit (HIRS)-2 channels 2–14, only Advanced Microwave Sounding Unit (AMSU)-A *NOAA-15* channels 3, 5, 7, and 9 and HIRS-3 *NOAA-17* channels 2–14, respectively, were assimilated. [The Community Radiative Transfer Model (CRTM) Stratospheric Sounder Unit (SSU) cell pressure correction noted in the "Use of the SSU in CFSR" section of Saha et al. (2010) was still in development while these tests were run.] The weight given to the new $(o - g)$ during the spinup is increased to 0.033 from the value of 0.00833 normally applied in the cycling of the assimilation system. The preliminary experiments show that the predictor coefficients, except for the CLW term, can start from zero and spin up rapidly, usually within 1 month (not shown). The coefficients for the CLW evolve very slowly, as shown in Fig. S23; thus, the CLW coefficients from *NOAA-15* are used as guess values of the training period for all the historical MSU channels.

Figures S24a–e show the global total bias (air mass plus scan angle) for the active channels of the AMSU-A *NOAA-15* and HIRS-3 *NOAA-17*. In these figures, CNTL

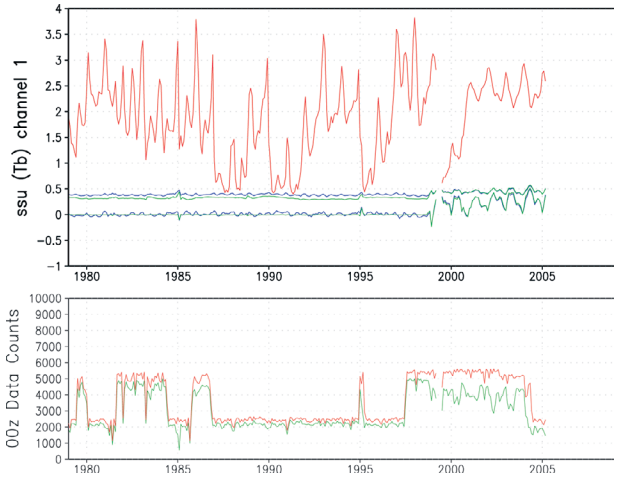

Fig. S19. As in Fig. S17, but for SSU channel 1, which peaks at ~ 15 hPa.

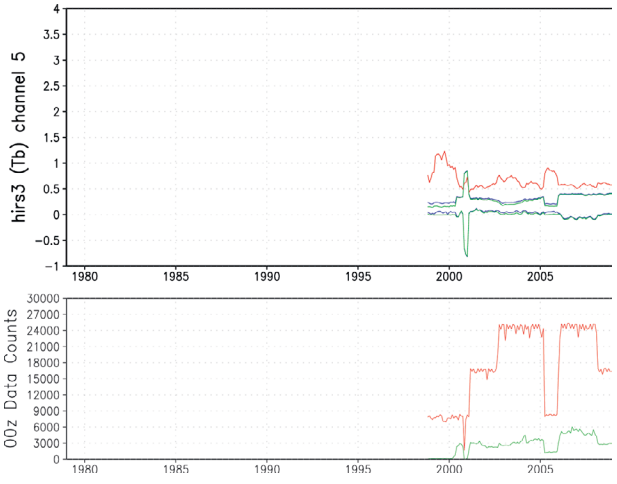

Fig. S20. As in Fig. S17, but for HIRS-3 channel 5, which peaks at ~ 500 hPa.

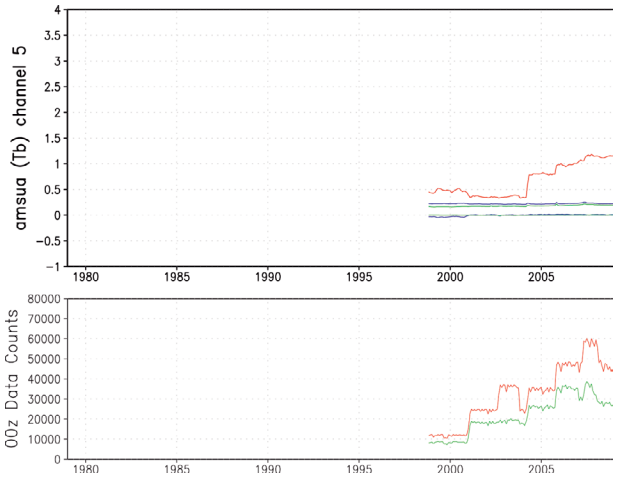

Fig. S21. As in Fig. S17, but for AMSU-A channel 5, which peaks at ~ 500 hPa.

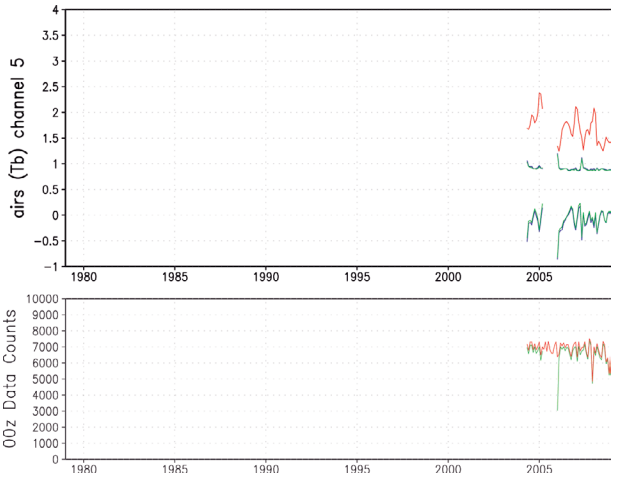

Fig. S22. As in Fig. S17, but for Atmospheric Infrared Sounder (AIRS) channel 215 (channel 92 in the 281 channel subset), which peaks ~ 450 hPa.

is the operational GDAS total bias for these channels as a reference. Most of the channels ($o-g$) equilibrate within about 1 month, except for HIRS-3 *NOAA-17* channel 12, which took about 2.5 months. Therefore, the training length for all the historical satellites was chosen to be 3 months.

The next prerequisite to running the spinup experiments was to assemble a time series of active channels and sensors for all the historical satellites, the SATINFO files, marked with periods of known outages and poor quality data. The starting point was a set of tables and scripts received, via the Joint Center for Satellite Data Assimilation (JCSDA) collaboration, from the Modern Era Retrospective-Analysis for Research and Applications (MERRA) reanalysis (see Bosilovich 2008). The tables and scripts were updated based upon the 40-yr European Centre for Medium-Range Weather Forecasts (ECMWF) Reanalysis (ERA-40) quality control list and the NCEP historical satellite document (maintained by D. Keyser online at www.emc.ncep.noaa.gov/mmb/data_processing/Satellite_Historical_Documentation.htm).

Once a working set of SATINFO files were created [and the historical set of SSU instruments were included in the CRTM, as noted in "Use of the SSU in the CFSR" of Saha et al. (2010)], a set of bias correction spinup experiments, listed in Table S2, was carried out by running the CFSR over the indicated 3-month periods when the satellite data first became available (see Fig. 4 of Saha et al. 2010). In two cases, *NOAA-6* and *-11* operated during two periods, so the bias correction spinup had to be done twice. Once each spinup experiment was complete, the postprocessing step was carried out on the ($o-g$) diagnostic files to create the initial SATANG files; it was then paired with the BIASCR file from the last cycle of the training period for use when the final CFSR assimilation began assimilating that particular instrument and sensor. Two features of this bias correction scheme should be noted. One is that the scan angle–dependent bias is the dominant part of the total bias, and the other is the predictor coefficients of the airmass bias usually responds to the atmospheric state very quickly, usually within 1 or 2 days.

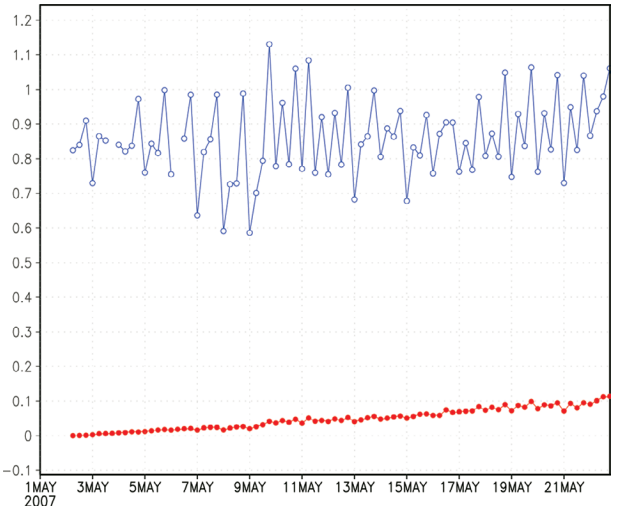

Fig. S23. The cloud liquid water bias term for AMSU-A *NOAA-15* channel 3 varies with time during 2007042218–2007052218. The red curve is initialized from zero and the blue curve represents the operational values used as a reference here.

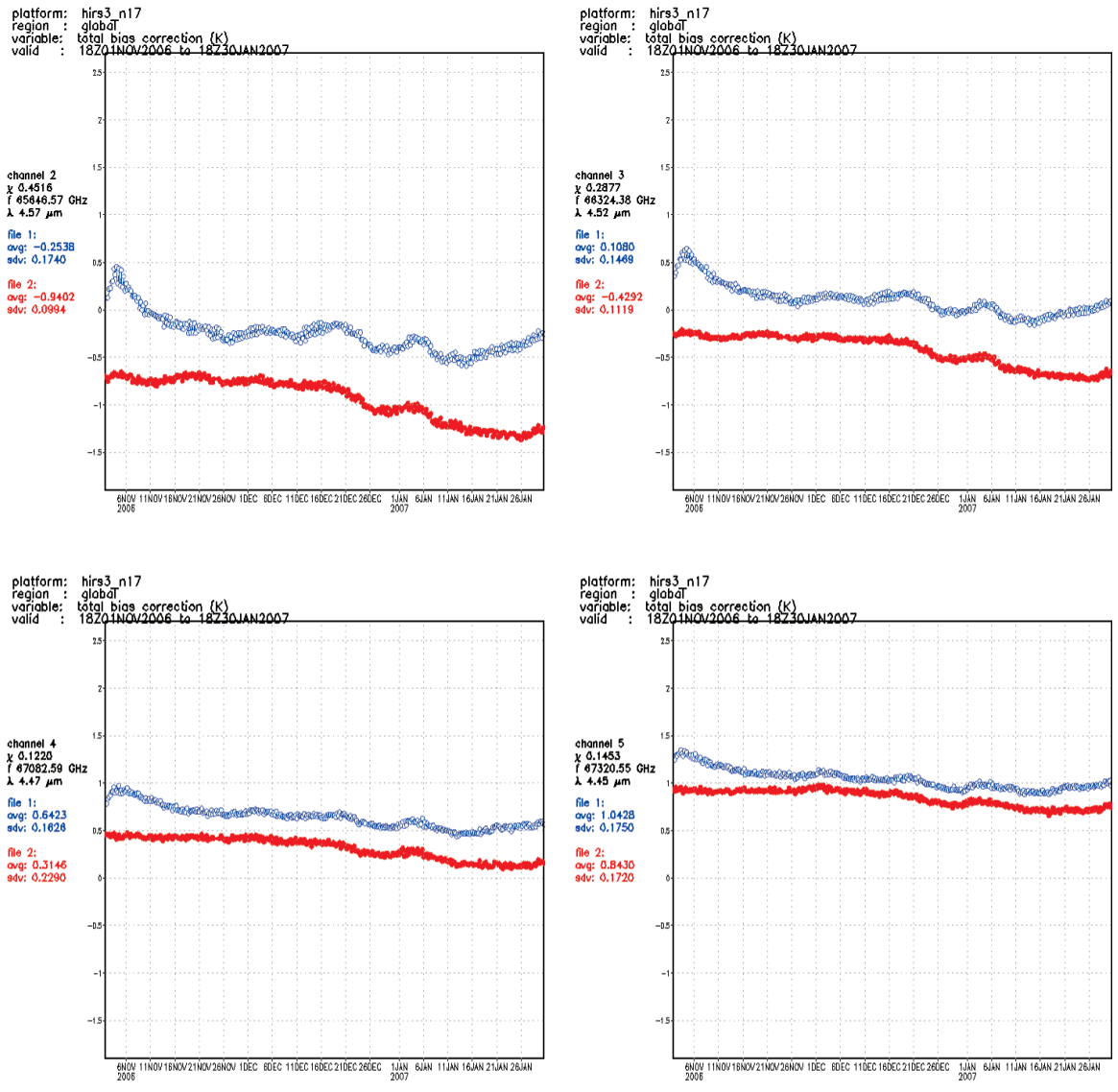

FIG. S24(a). The global total bias for HIRS-3 *NOAA-17* channels 2–5, which varies with time during 2006110118–2007013018. The blue curve is the experiment values and the red curve is the operational values used as a reference.

THE DATA ACCESS. To address a growing need for remote access to high-volume numerical weather prediction and global climate models and data, NOAA's National Climatic Data Center (NCDC), along with NCEP and the Geophysical Fluid Dynamics Laboratory (GFDL), initiated the NOAA Operational Model Archive and Distribution System (NOMADS; Rutledge et al. 2006) project. The NOMADS framework was developed to facilitate climate model and observational data intercomparison capabilities as discussed in documents such as the work of the Intergovernmental Panel on Climate Change (Houghton et al. 2001), and advances a direct recommendation by the National Academies of Science, Board on Atmospheric Sciences and Climate (BASC) to improve multimodel ensemble diagnostics capabilities (National Research Council 2007).

Of the 380-TB CFSR total output (estimated at the time of this writing), approximately 10 TB are considered to be the "tier 1" or "high-priority" data. These data were determined by several requirements workshops conducted by NCEP and at an NCDC-hosted Reanalysis Town Hall Workshop at the January 2008 Annual Meeting of the American Meteorological Society (AMS). At the AMS meeting, NCDC obtained feedback on user requirements for this massive dataset. An outcome of that workshop culminated in the generation of a user Web page,

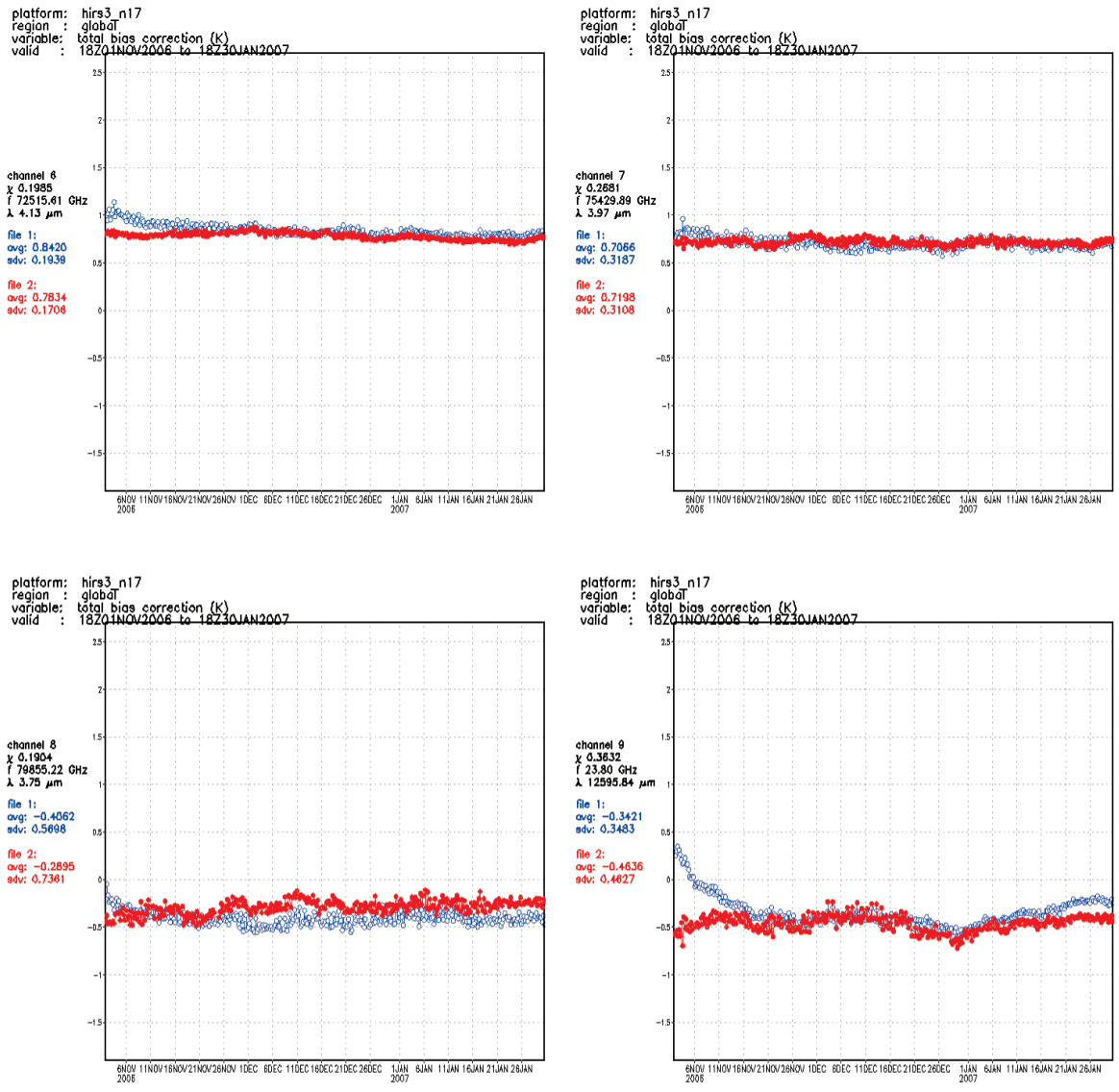

Fig. S24(b). As in Fig. S24(a), but for HIRS-3 *NOAA-17* channels 6–9.

soliciting additional user requirements. The NOAA Reanalysis Community Web Forum and can be accessed online (available at http://nomads.ncdc.noaa.gov/NOAAReanalysis/cfsrr).

The primary NOAA access point for CFSR is NCDC NOMADS (online at http://nomads.ncdc.noaa.gov/data.php?name=access#cfsr). NOMADS data access to CFSR is facilitated by file and variable-type organization most requested by users based on previous reanalysis outputs. The Tier 1 data include a suite of variables aggregated in a long time series, and a suite of monthly mean variables. The monthly mean and time series data are available as separate files by variable type, month, and year for the period of record to facilitate user access. A separate dataset of monthly mean data have been aggregated for access as individual files of a specific type so users can make a single request for the entire period of record of individual variables (e.g., 31 years of 500-hPa heights). These "long time series" datasets will greatly reduce processing time on the NCDC NOMADS while also providing improved user access response times.

To facilitate user access, the National Center for Atmospheric Research (NCAR) has agreed to act as a mirror site to the NCDC's NOMADS access point and is scheduled to provide access to CFSR. (The NCAR access point is http://dss.ucar.edu/pub/cfsr.html). Given the massive volume of these data, users are cautioned that extremely high-volume data requests may be throttled at NCDC based on the size of the individual request and the number of concurrent users.

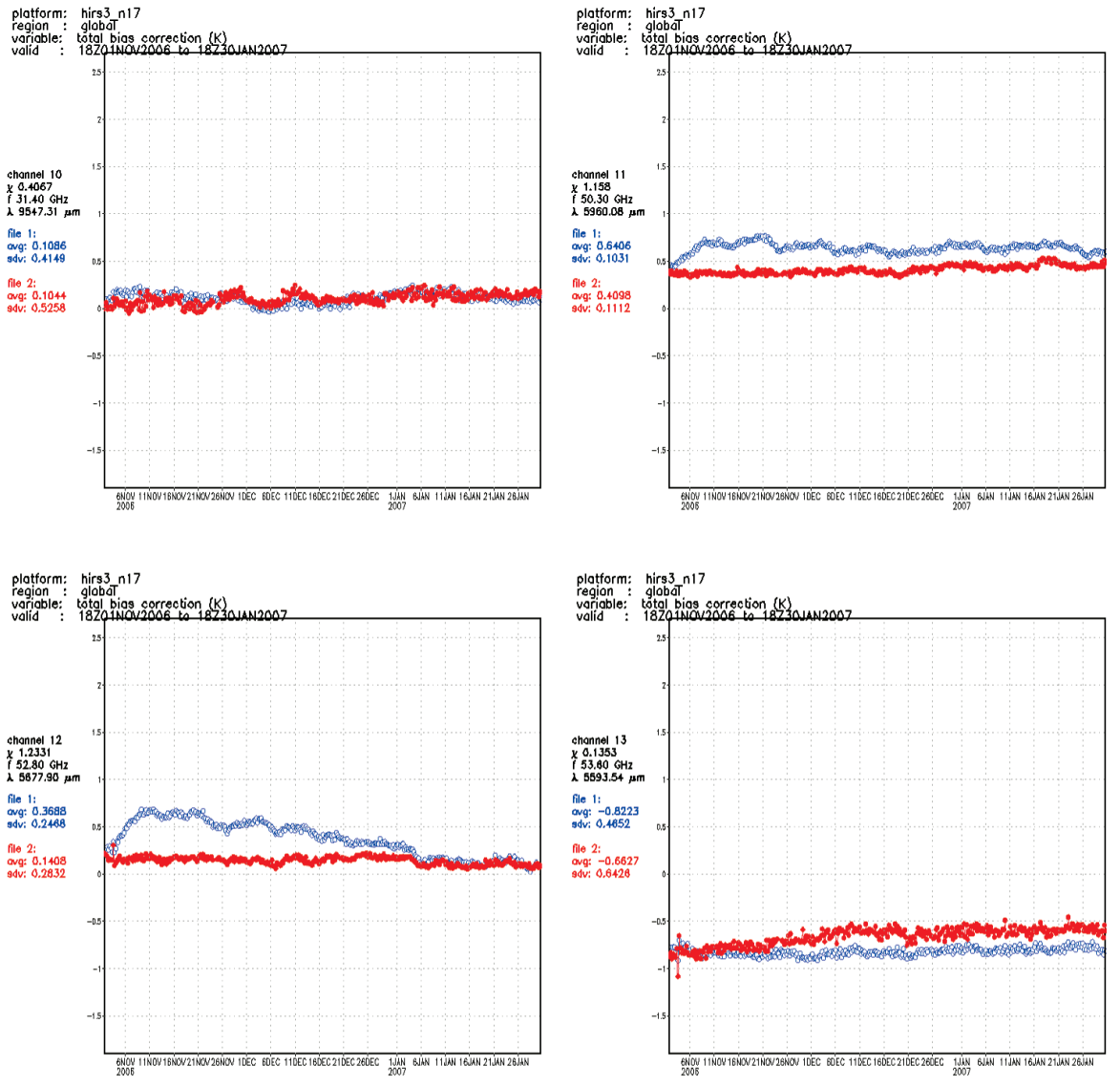

FIG. S24(c). As in Fig. S24(a), but for HIRS-3 *NOAA-17* channels 10–13.

REFERENCES

Bosilovich, M., 2008: NASA's modern era retrospective-analysis for research and applications: Integrating Earth observations. *Earthzine,* 26 September 2008. [Available online at www.earthzine.org/2008/09/26/nasas-modern-era-retrospective-analysis/.]

Derber, J. C., and W.-S. Wu, 1998: The use of TOVS cloud-cleared radiances in the NCEP SSI analysis system. *Mon. Wea. Rev.,* **126,** 2287–2299.

Houghton, J. T., Y. Ding, D. J. Griggs, M. Noguer, P. J. van der Linden, X. Dai, K. Maskell, and C. A. Johnson, 2001: *Climate Change 2001: The Scientific Basis.* Cambridge University Press, 944 pp.

National Research Council, 2007: *Completing the Forecast: Characterizing and Communicating Uncertainty for Better Decisions Using Weather and Climate Forecasts.* National Academies of Science, 76 pp.

Rutledge, G. K., J. Alpert, and W. Ebuisaki, 2006: NOMADS: A climate and weather model archive at the National Oceanic and Atmospheric Administration. *Bull. Amer. Meteor. Soc.,* **87,** 327–341.

Saha, S., and Coauthors, 2010: The NCEP climate forecast system reanalysis. *Bull. Amer. Meteor. Soc.,* **91,** 1015–1057.

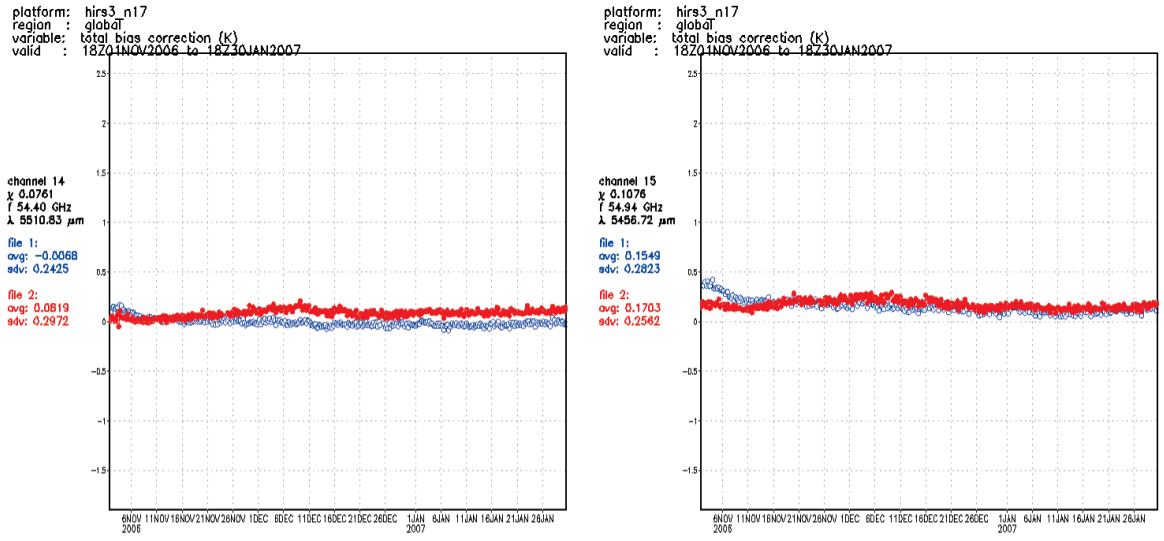

Fig. S24(d). As in Fig. 24(a), except for HIRS-3 *NOAA-17* channels 14 and 15.

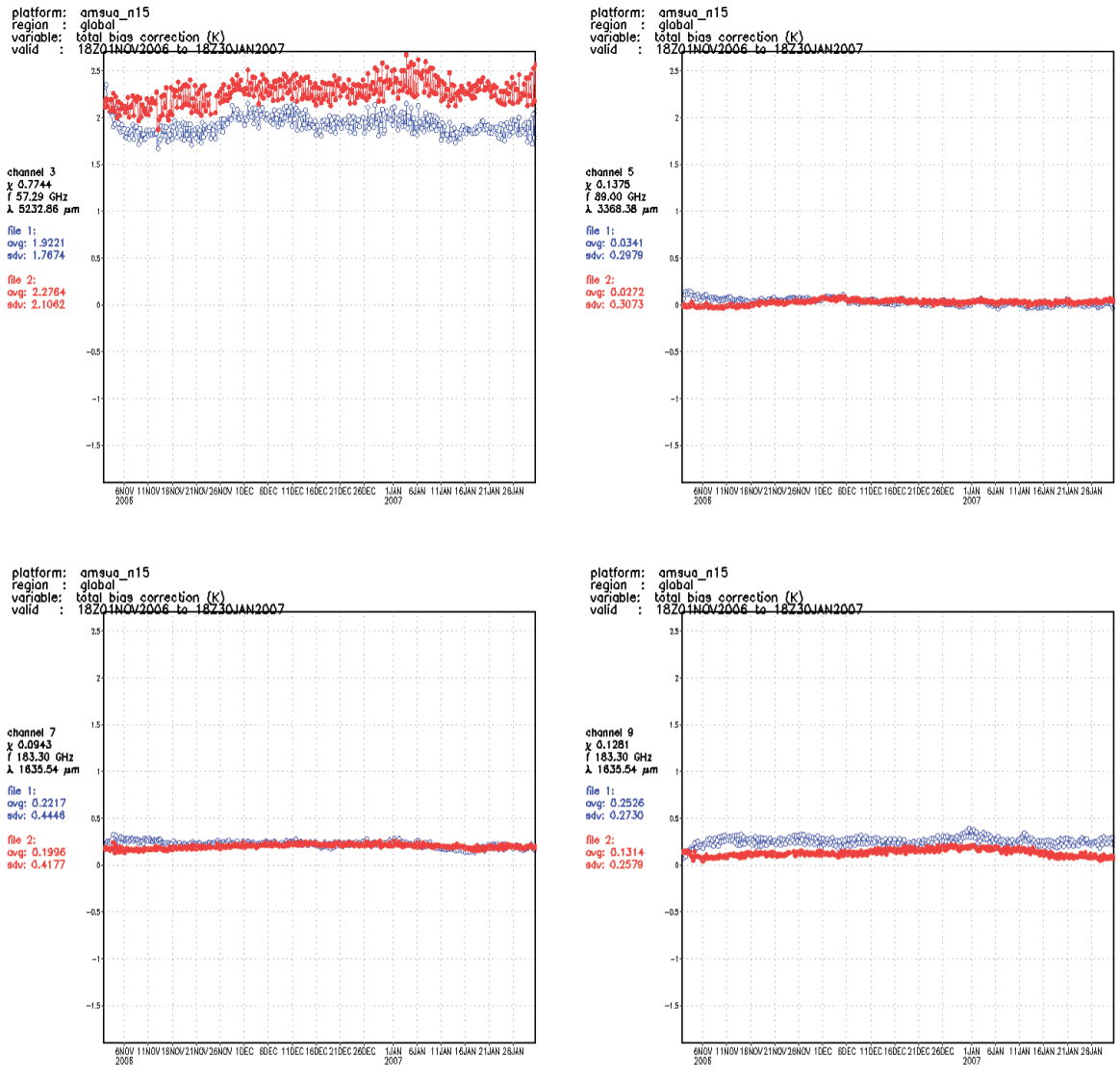

Fig. S24(e). As in Fig. S24(a), but for AMSU-A *NOAA-15* channels 3, 5, 7, and 9.

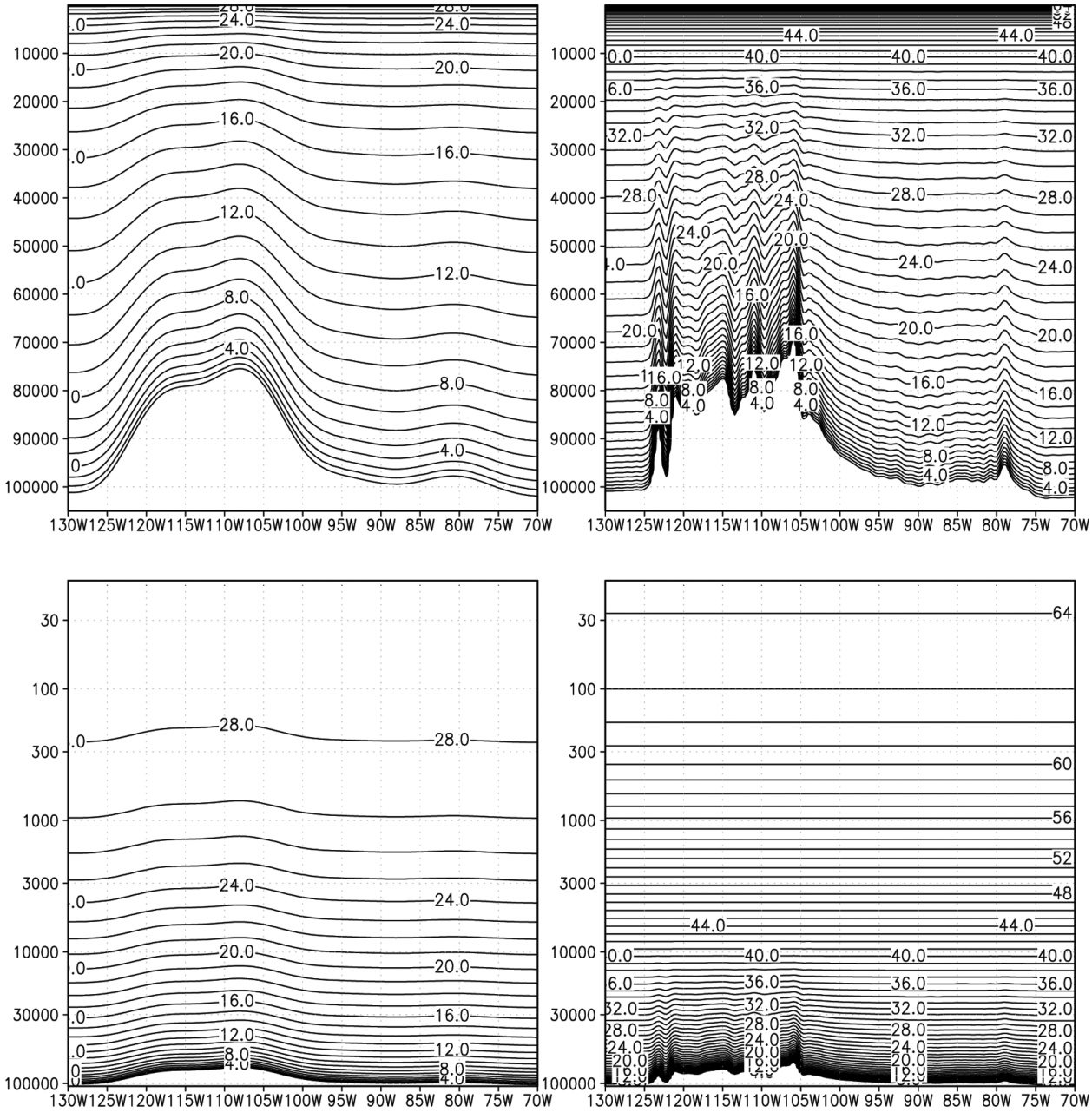

Fig. S25. The vertical structure of model levels as a zonal cross section across the Rockies at 40°N. (left) NCEP/NCAR Reanalysis Global Reanalysis 1 (R1; 28 sigma layers) and (right) CFSR (64 sigma–pressure hybrid layers). Plotted (top) as a linear function of pressure to emphasize resolution in the troposphere and (bottom) in log(pressure) to emphasize the stratosphere.

APPENDIX: THE DATA DESCRIPTION

Table SA1. Monthly means (0000, 0600, 1200, and 1800 UTC, and daily averages analysis with 0–6-h forecast).

File	Grid	Description	MB/month
FLXF	T382	Surface, radiative fluxes, etc.	3,500
FLXL	T62		105
PGBH	1/2°	3D pressure level data	11,200
PGBL	2.5°		480
OCNH	1/2°	3D ocean data	2,100
OCNF	1°		570
DIABF	1°	Diabatic heating, etc.	2,400
DIABL	2.5°		525
IPVH	1/2°	3D isentropic level data	2,200
IPVL	2.5°		100
EGYH	1/2°	Energetics, $u'v'$, TKE, etc.	7,100
EGYL	2.5°		280

Table SA2. Hourly time series from FLX files (32 parameters): low-resolution (T62 Gaussian) and high-resolution (T382 Gaussian).

File	Description	Low/high resolution (MB month^{-1})
DLWSFC	Downward LW at the surface	40/605
DSWSFC	Downward SW at the surface	26/360
GFLUX	Ground heat flux	7/168
ICECON	Ice concentration	5/56
ICETHK	Ice thickness	5/103
LHTFL	Latent heat flux	12/215
PRATE	Precipitation rate	12/208
PRESSFC	Surface pressure	18/295
PWAT	Precipitable water	14/190
Q2M	2-m specific humidity	21/444
RUNOFF	Ground runoff	9/159
SHTFL	Sensible heat flux	12/208
SNOHF	Snow phase-change heat flux	3/77
SOILM1	Soil moisture level 1	8/230
SOILM2	Soil moisture level 2	8/230
SOILM3	Soil moisture level 3	8/230
SOILM4	Soil moisture level 4	8/230
SOILT1	Soil temperature level 1	11/284
SWE	Snow-water equivalent	12/81
TMAX	Maximum 2-m air temperature	11/171
TMIN	Minimum 2-m air temperature	11/171
TMP2M	2-m air temperature	24/473
TMPHY1	Temperature at hybrid level 1	26/470
TMPSFC	Surface temperature	24/477
U10M	*U* at 10 m	36/633
V10M	*V* at 10 m	(UV combined)
UFLX	*U* stress	29/491
VFLX	*V* stress	(UV combined)
ULWSFC	Upward LW at the surface	10/153
ULWTOA	Upward LW at the top	12/187
USWSFC	Upward SW at the surface	7/101
USWTOA	Upward SW at the top	9/154

Table SA3. Hourly time series from PGB files (27 parameters): low-resolution (2.5°) and high resolution (0.5°).

File	Description	Low/high resolution (MB month^{-1})
CHI200	Velocity potential at 200 hPa	7/73
CHI850	Velocity potential at 200 hPa	7/73
PRMSL	Mean sea level pressure	18/230
PSI200	Streamfunction at 200 hPa	9/82
PSI850	Streamfunction at 850 hPa	9/88
Q500	Specific humidity at 500 hPa	11/202
Q700	Specific humidity at 700 hPa	8/150
Q850	Specific humidity at 850 hPa	8/157
Q925	Specific humidity at 925 hPa	9/153
T1000	Temperature at 1000 hPa	5/85
T2	Temperature at 2 hPa	5/51
T200	Temperature at 200 hPa	5/61
T50	Temperature at 50 hPa	5/52
T500	Temperature at 500 hPa	5/68
T700	Temperature at 700 hPa	5/79
T850	Temperature at 850 hPa	5/86
VVEL500	Vertical velocity at 500 hPa	12/306
WND200	*U* and *V* wind at 200 hPa	15/202
WND500	*U* and *V* wind at 500 hPa	20/360
WND700	*U* and *V* wind at 700 hPa	20/393
WND850	*U* and *V* wind at 850 hPa	20/400
WND1000	*U* and *V* wind at 1000 hPa	20/384
Z200	Geopotential at 200 hPa	13/161
Z500	Geopotential at 500 hPa	13/175
Z700	Geopotential at 700 hPa	16/200
Z850	Geopotential at 850 hPa	17/206
Z1000	Geopotential at 1000 hPa	18/221

Table SA4. Hourly time series from OCN files (13 parameters): low resolution (1°) and high resolution (0.5°).

File	Description	Low/high resolution (MB month^{-1})
OCNDT20C	Depth of 20°C isotherm	15/50
OCNHEAT	Ocean heat content	55/155
OCNMLD	Ocean mixed layer depth	27/95
OCNSAL5	Ocean salinity at depth of 5 m	23/75
OCNSAL15	Ocean salinity at depth of 15 m	23/75
OCNSLH	Sea level height	34/118
OCNSST	Ocean potential temperature at depth of 5 m	34/118
OCNT15	Ocean potential temperature at depth of 15 m	34/118
OCNU5	Ocean zonal current at depth of 5 m	36/130
OCNV5	Ocean meridional current at depth of 5 m	36/130
OCNU15	Ocean zonal current at depth of 15 m	36/130
OCNV15	Ocean meridional current at depth of 15 m	36/130
OCNVV55	Ocean vertical velocity at depth of 55 m	72/212

Table SA5. Hourly time series from IPV files (three parameters): low resolution (2.5°) and high resolution (0.5°).

File	Description	Low/high resolution (MB month^{-1})
IPV450	Potential vorticity at 450-K isentropic	11/140
IPV550	Potential vorticity at 550-K isentropic	11/140
IPV650	Potential vorticity at 650-K isentropic	11/140

Table SA6. Six-hourly output archives.

Type	Description	Output files	Per file MB
FLXF	104 records, sfc, radiative flux vars	f00–f06, f09	30
PGBH	628 records, pressure level vars	anl, f00–f06, f09	90
OCNH	222 records, ocean variables	f01–f06, f09	35
DIABF	926 records, diabatic heating, etc.	f00–f06, f09	26
IPVH	130 records, isentropic level	anl, f00–f06, f09	17

Table SA7. Initial conditions archive; low- and high-resolution approximate file size.

File	Description	Low/high resolution (MB)
SIGANL	3D hybrid analysis (binary)	230/25
SIGF00	3D hybrid one time-step forecast (binary)	230/25
SIGF06	3D hybrid 6-h forecast (binary)	230/25
SFCANL	Surface analysis (binary)	120/13
SIGF00	Surface one time-step forecast (binary)	120/13
SIGF06	Surface 6-h forecast (binary)	120/13
OCNANL	Ocean analysis (binary)	1250 (high-resolution only)